Global Change Biology (2004) **10,** 1470–1481, doi: 10.1111/j.1365-2486.2004.00829.x

Dynamics of carbon stocks in soils and detritus across chronosequences of different forest types in the Pacific Northwest, USA

OSBERT J. SUN*, JOHN CAMPBELL†, BEVERLY E. LAW† and VERNON WOLF†
*Laboratory of Quantitative Vegetation Ecology, Institute of Botany, the Chinese Academy of Sciences, Beijing 100093, China,
†Department of Forest Science, College of Forestry, Oregon State University, Corvallis, OR 97331, USA

Abstract

We investigated variation in carbon stock in soils and detritus (forest floor and woody debris) in chronosequences that represent the range of forest types in the US Pacific Northwest. Stands range in age from <13 to >600 years. Soil carbon, to a depth of 100 cm, was highest in coastal Sitka spruce/western hemlock forests ($36 \pm 10\,kg\,C\,m^{-2}$) and lowest in semiarid ponderosa pine forests ($7 \pm 10\,kg\,C\,m^{-2}$). Forests distributed across the Cascade Mountains had intermediate values between 10 and $25\,kg\,C\,m^{-2}$. Soil carbon stocks were best described as a linear function of net primary productivity ($r^2 = 0.52$), annual precipitation ($r^2 = 0.51$), and a power function of forest floor mean residence time ($r^2 = 0.67$). The highest rates of soil and detritus carbon turnover were recorded on mesic sites of Douglas-fir/western hemlock forests in the Cascade Mountains with lower rates in wetter and drier habitats, similar to the pattern of site productivity. The relative contribution of soil and detritus carbon to total ecosystem carbon decreased as a negative exponential function of stand age to a value of ~35% between 150 and 200 years across the forest types. These age-dependent trends in the portioning of carbon between biomass and necromass were not different among forest types. Model estimates of soil carbon storage based on decomposition of legacy carbon and carbon accumulation following stand-replacing disturbance showed that soil carbon storage reached an asymptote between 150 and 200 years, which has significant implications to modeling carbon dynamics of the temperate coniferous forests following a stand-replacing disturbance.

Keywords: carbon stock, chronosequence, climate, disturbance, forest ecosystem, soil carbon

Received 21 May 2003; revised version received 4 March 2004; accepted 8 March 2004

Introduction

Soil and plant detrital carbon are significant components of terrestrial ecosystems and sources of heterotrophic respiration. The rates of their accumulation and turnover not only determine the changes in carbon storage, but also control net ecosystem productivity (Janisch & Harmon, 2002; Law *et al*., 2003). Quantifying the dynamics of soil and detrital carbon accumulation and turnover is important for elucidating the role of forest ecosystems in the global carbon cycle.

Carbon storage and turnover vary spatially and temporally under the influence of climate, management, and disturbance (Giardina & Ryan, 2000; Rustad *et al*., 2001; Schuur *et al*., 2001; Guo & Gifford, 2002). Catastrophic fire and forest harvesting are common disturbances resulting in significant changes in carbon stocks and fluxes in forest ecosystems (Law *et al*., 2003; Wang *et al*., 2003), but their effects on soil carbon are less understood. It has been suggested that forest harvesting may have relatively little effect on soil carbon (Johnson & Curtis, 2001). Given their different dynamics, there is generally agreement that it is critical to distinguish between labile and nonlabile pools in mineral soils (Davidson *et al*., 2000). Neff *et al*. (2002) reports, for example, that nitrogen additions significantly accelerated turnover of the labile (light density fractions) of soil carbon, but reduced turnover rates of the less labile (heavy density fractions) more closely bound to mineral soil particles. As a result, total

Correspondence: O. J. Sun, e-mail: osbertsun@ibcas.ac.cn

soil carbon remained unchanged (Neff *et al.*, 2002). Detrital carbon is predominantly a labile pool of ecosystem carbon with yearly or decadal turnover times.

The rate of soil carbon accumulation and turnover is difficult to assess, even with sophisticated simulation methods (Eswaran *et al.*, 1993; Parton *et al.*, 1995; Torn *et al.*, 1997; Homann *et al.*, 1998). The total soil carbon pool, however, can be estimated from detailed analysis of carbon content through the soil profile. Such analysis, while laborious and costly, can provide basic information for estimating and modeling regional soil carbon storage in relation to land use and land cover, as well as for assessing the impact of climate change on soil carbon dynamics.

In this paper, we provide detailed analysis of the rate at which carbon in mineral soils and detritus accumulates and turns over across chronosequences of a wide range of forest types in the US Pacific Northwest. The objectives of our study were to determine: (1) variation of carbon stocks and fluxes in soils and various detrital pools as influenced by climate and forest types, and (2) dynamics of soil and detrital carbon accumulation and turnover following stand-replacing disturbance in temperate coniferous forest ecosystems of the Pacific Northwest.

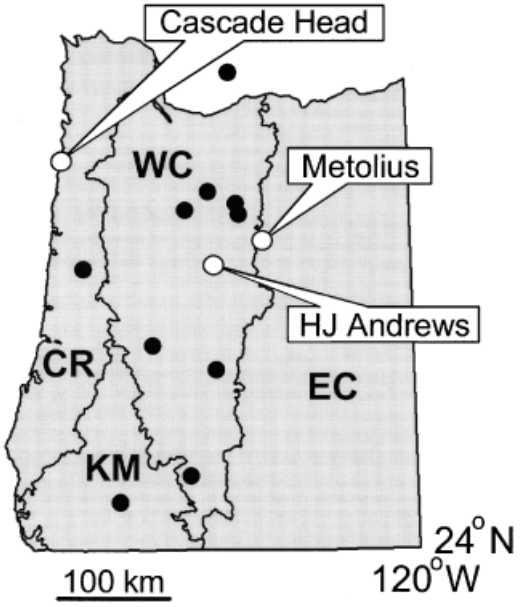

Fig. 1 Geographic locations of study sites and ecoregions in Oregon and southern Washington. Block dots show locations of extensive sites. Ecoregions: CR, Coast Range; WC, West Cascades; EC, East Cascades; KM, Klamath Mountains. Based on the boundaries defined in Franklin & Dyrness (1973).

Materials and methods

Study design and definitions

In total, 13 separate chronosequences were established throughout western Oregon and southern Washington (Fig. 1). Ten of these chronosequences (extensive sites) were distributed throughout a multidimensional climate space west of the Cascade Mountains (Law *et al.*, 2004). Three of these chronosequences (intensive sites) were designated for intensive measurement and were located across a steep precipitation gradient from the cool and wet forests of the Pacific Coast Range (Cascade Head (CH) site) to the montane forests of the west Cascades (Andrews (HJ) site) to the semiarid forests of the east Cascades (Metolius (ME) site). Species composition of each study site is given in Table 1. The chronosequences at the intensive sites were comprised of twelve 1 ha plots arranged as three replicates of four developmental stages (initiation, young, mature, and old). The developmental stages were categorized arbitrarily based on contrasting growth and structural characteristics of the stands, and were represented by different age ranges for different forest types. The chronosequences at the extensive sites were comprised of six 1 ha plots representing each of six age classes ($<$13, 13–29, 29–50, 50–100, 100–200, and $>$200 years following stand-replacing disturbance). With plots stratified randomly within climate space, forest type and forest age, their specific locations are random with respect to slope, aspect, landform, and soil series. Given that the extensive sites were sampled without replication, we pooled the data by age classes across the 10 sites to examine the temporal dynamics of soil and detrital carbon stocks (Law *et al.*, 2004).

In this study, we use the term soil carbon to refer to the organic carbon present in the mineral soil exclusive to that present in the forest floor (soil O-horizon), roots, and root symbionts. The term detritus is used to refer to all dead organic tissue in the form of forest floor, fine woody debris (FWD), and coarse woody debris (CWD) (including stumps, standing snags, and their associated coarse roots). The term necromass refers collectively to soil and detritus carbon and distinguishes this total dead organic matter from all living biomass.

Estimates of long-term average annual precipitation and annual mean air temperature were derived from the climate map of Oregon created using PRISM developed by Chris Daly of Oregon State University and George Taylor of the Oregon Climate Service at Oregon State University (www.ocs.orst.edu/prism/prism_new.html) based on the coordinates and elevations of the plots.

Biomass and net primary productivity (NPP)

As part of a research program on scaling ecosystem carbon fluxes in the Pacific Northwest (Law *et al.*, 2004),

Table 1 Locations and tree species composition across the 13 study sites in the Pacific Northwest

Site ID	Location name	Ecoregion	Latitudinal range	Longitudinal range	Elevational range (m)	Major tree species*
Intensive sampling sites						
CH	Cascade Head, Oregon	Coast Range	45°03′–07′N	123°52′–55′W	120–325	Tshe > Psme > Pisi > Alru
HJ	HJ Andrews LTER site, Oregon	West Cascades	44°14′–16′N	122°10′–14′W	700–860	Psme > Tshe > Thpl > Cach
ME	Metolius, Oregon	East Cascades	44°25′–30′N	121°33′–40′W	880–1235	Pipo > Cade
Extensive sampling sites						
LM	Lookout Mountain, Washington	West Cascades	45°49′–52′N	122°01′–07′W	570–1200	Abam > Psme > Abpr > Tshe
BH	Breitenbush Hot Springs, Oregon	West Cascades	44°46′–48′N	121°53′–122°00′W	835–1450	Psme > Abam > Tshe > Pico > Tsme
BA	Battle Ax, Oregon	West Cascades	44°47′–50′N	122°09′–15′W	745–1285	Psme > Tshe > Abam > Thpl
MJ	Mount Jefferson, Oregon	West Cascades	44°41′–42′N	121°52′–53′W	1080–1220	Psme > Tshe > Abam > Abpr
MC	Mill City South, Oregon	West Cascades	44°38′–44′N	122°23′–30′W	460–1035	Tshe > Psme > Alru > Acma
HR	Hellion Rapid, Oregon	Coast Range	44°24′–29′N	123°47′–52′W	340–620	Psme
BM	Blue Mountain, Oregon	West Cascades	43°41′–44′N	122°54′–56′W	450–880	Psme > Tshe > Thpl
EB	Emigrant Butte, Oregon	West Cascades	43°25′–30′N	122°10′–15′W	1210–1490	Psme > Abpr > Tshe > Abgr > Tsme
BB	Big Butte Springs, Oregon	West Cascades	42°34′–37′N	122°24′–30′W	830–1030	Psme > Abgr > Pipo > Cade
GP	Grants Pass, Oregon	Klamath Mts	42°28′–30′N	123°16′–18′W	725–970	Psme > Arme > Cade

*Species with greater than 5% presence. ID: Abam, *Abies amabilis*; Abpr, *Abies procera*; Abgr, *Abies grandis*; Acmc, *Acer macrophyllum*; Alru, *Alnus rubra*; Arme, *Arbutus menziesii*; Cade, *Calocedrus decurrens*; Pico, *Pinus contorta*; Pipo, *Pinus ponderosa*; Psme, *Pseudotsuga menziesii*; Thpl, *Thuja plicata*; Tshe, *Tsuga heterophylla*; Tsme, *Tsuga mertensiana*.

we estimated carbon stocks in soils and detritus, above- and belowground biomass, and productivity at both the intensive and extensive study plots. Net primary productivity (NPP) was determined from measurements of tree and shrub dimensions, radial growth increment, species-specific plant volume equations, and species-specific wood density values developed for the region. Details of the measurements leading to biomass and NPP are given in Law *et al*. (2003, 2004).

Soil carbon stocks

Measurements of soil carbon and nitrogen concentrations, as well as texture, were made on six soil cores (7.6 cm diameter), on each plot at the intensive sites, and three cores at the extensive sites, separated into 0–20, 20–50, and 50–100 cm layers. All samples were transported to a laboratory within 3 days of collection, and stored in a refrigerated storage room before being air-dried in a ventilation drying system. After removing live vegetation and roots, the air-dried samples were pulverized and analyzed for total carbon and nitrogen with a LECO CNS 2000 analyzer (LECO Corporation, St Joseph, MI, USA). Soil bulk density was estimated as the total dry mass of the sample divided by the volume of the core sample. The dry mass of the sample included stones that were uncommon in the cores. Soil texture was determined by the specification hydrometer method (Gee & Bauder, 1986), with the particle sizes classified into sand (50–2000 μm), silt (2–50 μm), and clay (<2 μm). Carbon content in soils was calculated for each soil layer from layer depth, bulk density, and percent organic carbon data, and summed for all layers to estimate total carbon content to 100 cm depth.

Forest floor mass and turnover

Mean residence time of the forest floor was calculated by dividing the forest floor mass by the annual litterfall rate for each plot. This method assumes equilibrium between litterfall input and forest floor decomposition.

Six samples of forest floor were collected on each plot at all sites. Samples consisted of dead plant material with identifiable tissue structure less than 1 cm in diameter, including foliage, twigs, and tissues of herbaceous plants. After drying at 70 °C for 48 h, the samples were weighed to determine mass, and analyzed for carbon and nitrogen concentrations with a LECO CNS 2000 analyzer.

At the intensive plots, annual litterfall rate from trees and understory shrubs was estimated with eight regularly distributed 1.6 m^2 collection traps. At the extensive sites, annual litterfall rate from trees and understory shrubs was estimated as the mass of tree and understory foliage divided by the mean foliage

retention age on each plot. Tree foliage biomass was calculated from estimates of leaf area index and a weighted average of specific leaf area for each plot while understory foliage biomass was determined allometrically from dimensional measurements for shrubs and by clippings of herbaceous plants on the ground (Law *et al*., 2003).

Annual litter fall from herbaceous plants is considered to equal the live mass of the plants (with an annual life cycle of the aboveground tissues), which was determined for each plot from four regularly distributed 3–12 m^2 clip plots. In all cases, the carbon concentration of litter fall was assumed to be 50% of its dry mass.

Woody debris mass and decomposition

Carbon in woody debris was measured for the coarse fragments (CWD > 10 cm diameter, and > 1 m length) for all the plots, and fine fragments (FWD = 1–10 cm diameter) for the intensive sites only following Harmon & Sexton (1996). Annual carbon loss from CWD (R_{hCWD}) and FWD (R_{hFWD}) decomposition was computed from mass per m^2 ground, and species-specific decay rates for the area. The detailed procedure of measurements and computations was described in Harmon & Sexton (1996) and Law *et al*. (2003).

Carbon in dead coarse roots (> 2 cm diameter) was estimated allometrically by using the coarse root biomass equations of Gholz *et al*. (1979). Coarse root biomass equations were converted to root volume equations. The volumetric conversions are necessary as wood density varies with species and with decay conditions, whereas the original coarse root biomass equations of Gholz *et al*. (1979) were for nondecayed roots. Basal and breast height (1.37 m) diameters of stumps and snags were used to obtain estimates of dead coarse root volumes, which were then converted to mass by using species-specific wood density of different decay classes (Harmon & Sexton, 1996). Carbon in dead, small (2–20 mm diameter), and fine (< 2 mm diameter) roots was determined using a soil coring method sampling to 100 cm depth as described by Law *et al*. (2003) at the intensive sites.

Soil respiration

Soil respiration was measured at 12 locations on each plot at the intensive sampling sites only for a full year at a bimonthly interval. Measurements were made on top of the forest floor with a portable soil respiration system (LI-6400 with LI-6000-9 soil chamber, LI-COR, Lincoln, NE, USA). Soil temperatures at 10 cm depth were measured simultaneously with a temperature probe (Model No. 8528-24, Cole-Parmer, Chicago, IL, USA) to develop plot-specific empirical relationships with soil respiration. Soil temperature was also measured continuously at 10 cm depth with temperature data logger (HOBO® Temp, Onset Computer Corporation, Bourne, MA, USA) for a full year at half-hourly time step for scaling monthly soil respiration measurements to annual carbon loss from soil.

Annual soil respiration was computed for each of the intensive plots following Ryan *et al*. (1997) and Law *et al*. (1999). This method involves the development of plot-specific temperature response curves, and then using soil temperature to model annual soil respiration. Specifically, daily average soil respiration was computed according to the following equation:

$$R_i = R_{i10} e^{(\beta T - 10)},$$

where R_i is the average soil respiration estimated for day i, R_{i10} is the average soil respiration for day i normalized to 10 °C (which is either a measured point or one linearly interpolated between measurements), β is from a season-wide temperature response curve $y = ae^{\beta x}$ (where y is the soil respiration and x the soil temperature), and T is the average soil temperature measured for day i.

Total soil respiration was partitioned into autotrophic (root systems) and heterotrophic respiration following the root separation method of Law *et al*. (2001). In spring, summer, and fall, soil respiration with and without forest floor was measured at 15 locations on each of the three plots representing initiation, young-, and old-growth stands at each intensive site. Following each flux measurement, the soil under the sample collar was cored to a depth of 30 cm and from these cores fine roots were quickly and carefully removed. The respiration of these roots was then measured in a dark chamber attached to the aforementioned IRGA and assumed to equal the contribution these roots made to the previously measured intact sample. This technique for the separation of heterotrophic and autotrophic contributions of total soil respiration is subject to error resulting from ambiguity of what truly represents autotrophic tissue. From our experience, this approach provides a good first estimate how much soil respiration can be attributed to roots vs. mineral soil. Based on these separation measurements, total annual soil respiration was partitioned into root, forest floor, and heterotrophic components to derive fraction of soil respiration attributable to root systems (Law *et al*., 2001).

Separation of light and heavy density fractions of soil carbon

Separation of the light (LF) and heavy (HF) carbon density fractions in mineral soils was conducted on

three composite samples of 18 soil cores on a subset of three plots representing distinct stages of stand development at intensive sites only. Each composite sample was made of equal portions of six sieved soil samples (<2 mm) on the same transect (0–20 and 20–50 cm depth).

The density fractionation was based on a modified suction method of Strickland & Sollins (1987). Carbon and nitrogen concentration of the LF materials were determined with a LECO CNS 2000 analyzer. Carbon mass of the HF material was calculated by subtracting LF carbon from the previously determined total soil carbon of each sample.

Modeling temporal dynamics of soil carbon storage

We simulated changes in soil carbon with stand age by considering two independent functional processes: (1) decomposition of legacy carbon (carbon stock immediately after stand-replacing disturbance), and (2) carbon accumulation from the current vegetation.

Decomposition of legacy soil carbon was modeled as two separate pools by an exponential decay function as

$$\mathrm{LC}_t = \mathrm{C}_0 \times \left[f(\mathrm{LF}) \times \mathrm{e}^{-k_\mathrm{D}(\mathrm{LF}) \times t} + f(\mathrm{HF}) \times \mathrm{e}^{-k_\mathrm{D}(\mathrm{HF}) \times t} \right],$$

where LC_t is the legacy carbon at time t following stand-replacement disturbance, C_0 is the initial total soil carbon, f(LF) and f(HF) are fractions of LF and HF carbon, and k_D(LF) and k_D(HF) are decomposition constants for LF and HF carbon. We derived k(LF) from the average estimates of soil carbon turnover rates determined for the intensive sites. The value of k(HF) was not known for any of our study sites. For our modeling purpose, we assumed the value of k(HF) to be 77% of k(LF) based on an incubation experiment of separated LF and HF material by Swanston *et al*. (2002). The actual value of k(HF) could differ due to recalcitrance and accessibility of HF organic material of undisturbed soils (Sollins *et al*., 1996).

Soil carbon accumulation following stand regeneration was modeled as a Chapman–Richards function:

$$\mathrm{AC}_t = \mathrm{C}_\mathrm{SS} \times \left(1 - \mathrm{e}^{-k_\mathrm{G} \times t}\right)^r,$$

where AC_t is the accumulation of carbon at time t, C_SS is the mean steady-state carbon pool, k_G is the growth constant, and r is the shaping parameter. We derived k_G and r by fitting a Chapman–Richards function to the total biomass carbon by stand age, and C_SS as the mean soil carbon stocks of old-growth stands (assumed equilibrium of soil carbon stock). Predicted soil carbon at time t (C_t) was given by

$$\mathrm{C}_t = \mathrm{LC}_t + \mathrm{AC}_t.$$

The model parameters fit to the equations above are given in Table 2.

Results

Spatial variation of carbon stock in soils and detritus

The 13 study sites varied widely in climate (Table 3). Long-term mean of annual precipitation ranges from ~ 500 mm in ponderosa pine forests at the ME site in central Oregon to ~ 3000 mm in Pacific silver fir (*Abies amabilis*) and Douglas-fir dominated forests at the Lookout Mountain (LM) site in southern Washington. Annual mean air temperature varies from ~ 6 °C at the Mount Jefferson (MJ) site to ~ 11 °C at the Hellion Rapids (HR) site.

Carbon stock in soil and the forest floor varied significantly ($P \leq 0.0001$) among sites. Spatially, soil carbon stock was the highest (~ 36 kg C m^{-2}) in mesic Sitka spruce and western hemlock forests at CH near the coast, the lowest (~ 7 kg C m^{-2}) in ponderosa pine at ME in the semiarid region of central Oregon, and ranged mostly from ~ 10 to ~ 25 kg C m^{-2} in forests of the Cascade Mountains (Table 4).

We found that, at the intensive sites, carbon stock in both soils and the total necromass increased with NPP (Fig. 2), and differed by about fivefold between the two extreme sites (CH and ME) along a gradient of site productivity (Table 5); as annual precipitation increased across sites, total soil carbon increased ($r^2 = 0.51$), and mean residence time of the forest floor decreased ($r^2 = 0.62$; Fig. 3); soil carbon decreased with mean residence time of the forest floor (Fig. 4). The mean residence time of the forest floor indicates both the rate of decomposition and carbon transfer from the forest floor to mineral soils.

Table 2 Model parameters of legacy soil carbon decomposition and soil carbon accumulation from current vegetation for the average of 10 extensive sites in the Pacific Northwest

Parameter	Value
Decomposition of legacy soil carbon, LC_t	
C_0 (g C m^{-2})	25 110
f(LF)	0.30
f(HF)	0.70
k_D(LF)	0.032
k_D(HF)	0.025
Soil carbon accumulation from current vegetation, AC_t	
C_SS (g C m^{-2})	19 400
k_G	0.016
r	1.55

Table 3 Climate and soil physical properties to a depth of 100 cm across the 13 study sites in the Pacific Northwest

Site	Annual precipitation (mm)*	Annual mean, T_{air} (°C)*	Soil bulk density ($g\,cm^{-3}$)†
Intensive sampling sites			
CH	2809 (137)b	10.5 (0.1)b	0.80 (0.04)efg
HJ	2096 (55)d	8.3 (0.2)d	0.97 (0.07)cde
ME	524 (57)h	7.4 (0.4)fg	1.18 (0.03)ab
Extensive sampling sites			
LM	3151 (198)a	7.8 (0.5)ef	0.85 (0.07)def
BH	1865 (106)e	7.1 (0.7)g	0.75 (0.06)fg
BA	2516 (196)c	8.1 (0.5)de	0.66 (0.03)fg
MJ	2033 (0)de	6.3 (0)h	0.74 (0.07)fg
MC	2112 (173)d	8.9 (0.3)c	1.06 (0.05)bc
HR	2819 (513)b	11.4 (0.5)a	0.72 (0.11)fg
BM	1447 (58)f	10.3 (0.3)b	1.00 (0.10)bcd
EB	1528 (83)f	6.9 (0.6)g	0.64 (0.06)g
BB	989 (40)g	9.3 (0.6)c	1.25 (0.06)a
GP	925 (43)g	10.4 (0.4)b	0.99 (0.10)bcde
$Pr > F$	0.0001	0.0001	0.0001

Standard deviations are shown in parentheses ($n = 12$ at the intensive sampling sites, and 6 at the extensive sampling sites). Values designated by the same letters are not significantly different at $P \leq 0.05$.
*Values of long-term average based on the climate map of Oregon created using PRISM (http://www.ocs.orst.edu/prism/prism_new.html).
†Average values for entire soil profile weighed by fraction of mineral soils and layer thickness.

Table 4 Soil and detrital carbon stocks ($g\,C\,m^{-2}$ ground) across 13 study sites in Pacific Northwest

Site	Soil C*	Forest floor C†	CWD C‡	Detrital CR_t C§
Intensive sampling sites				
CH	36 174 (10109)a	498 (169)c	2887 (1799)a	7396 (5458)a
HJ	14 244 (3112)defg	776 (284)bc	3083 (2325)a	1669 (1887)b
ME	7057 (2389)g	1408 (481)a	794 (490)a	1121 (1189)b
Extensive sampling sites				
LM	20 639 (5952)bcd	663 (449)bc	1875 (1782)a	1484 (745)b
BH	15 376 (5842)cdef	1140 (824)ab	1920 (1655)a	3643 (5033)ab
BA	20 126 (8996)bcd	1000 (432)abc	1570 (717)a	1632 (1340)b
MJ	24 660 (14677)b	924 (432)abc	1223 (–)a	1982 (1048)b
MC	22 861 (3941)bc	659 (256)bc	2900 (1986)a	–
HR	20 331 (5723)bcd	500 (308)c	771 (569)a	1283 (878)b
BM	17 118 (5234)bcde	762 (566)bc	1883 (1990)a	445 (387)b
EB	7992 (3033)fg	1002 (570)abc	1878 (929)a	2377 (3283)b
BB	14 515 (3422)defg	635 (307)bc	1320 (544)a	2198 (4224)b
GP	11 959 (3988)efg	910 (367)abc	1228 (779)a	1002 (1776)b
$Pr < F$	0.0001	0.0005	0.0330	0.0015

Standard deviations are shown in parentheses ($n = 12$ at the intensive sampling sites, and 6 at the extensive sampling sites). Values designated by the same letters are not significantly different at $P \leq 0.05$.
*Mineral Soil carbon to 100 cm depth
†Carbon in forest floor (leaves and plant tissue fragments on soil surface <1 cm diameter)
‡Carbon in coarse woody detritus pool (diameter >10 cm, length >1 m).
§Carbon in detrital coarse roots (>2 cm diameter) attached to snags and stumps.

Spatial and temporal dynamics of soil and detrital carbon

The average of the 10 extensive sites displayed a decline in soil carbon with stand age until ~ 50 years, followed by a slow recovery phase (Fig. 5). The same pattern was not observed at any of the intensive sites; there was no apparent age-related trend in soil carbon stock (Table 5) or annual heterotrophic respiration

(Table 6) in soils or detrital pools. It is difficult to point to any specific qualities of the intensive sites that would prevent them from conforming to the trends observed in the extensive sites. It is worth noting, however, that the extensive sites are located primarily in the western Cascades. As such, the only intensive site that is directly comparable is HJ and it may not be appropriate to expect any one site to conform to a trend based on regional data. Significant ($P \leq 0.05$) differences, however, were found among the three intensive sites in carbon stock in soils, forest floor, and total necromass. The soil and total necromass carbon were the highest under Sitka spruce and western hemlock forest types at the CH site near the coast, lowest under ponderosa pine forests at the semiarid ME site, and intermediate at the Douglas-fir/hemlock HJ site in the Cascades (Table 5). Heterotrophic respiration from various pools was similar between the CH and HJ sites, which were significantly ($P \leq 0.05$) greater than those at the ME site.

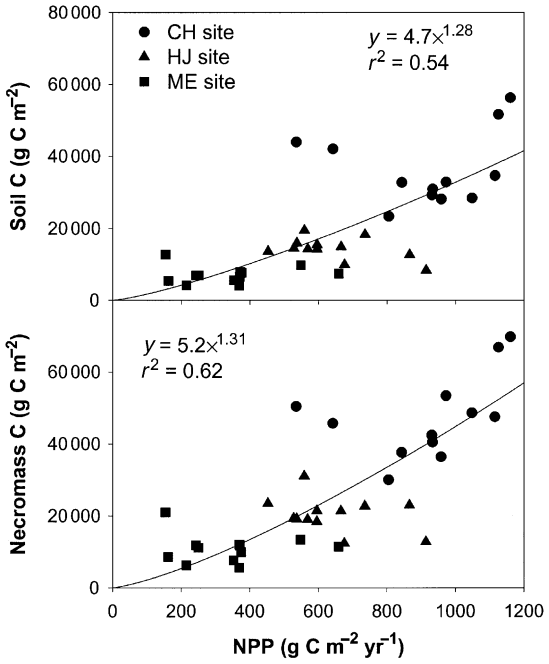

Fig. 2 Relationships between soil and necromass carbon stocks and net primary productivity (NPP) across 36 plots at the intensive sites in Oregon. The Cascade Head (CH), Andrews (HJ), and Metolius (ME) sites are located in the Coast Range, West Cascades, and East Cascades, respectively.

The relative contribution of total necromass carbon to ecosystem carbon decreased as a result of increasing biomass with stand age. Rates of decrease in the ratio of total necromass carbon to ecosystem carbon with stand age followed the same trend among the three intensive sampling sites that vary markedly in climate and forest types (Fig. 6). Climate and forest type had no impact on the partitioning of carbon stock between biomass and necromass as a function of stand age. The relative contribution of total necromass carbon to ecosystem carbon appeared to approach an asymptote of $\sim 35\%$ between 150 and 200 years.

The annual turnover rate of necromass carbon, which is defined as total necromass carbon over total heterotrophic respiration, increased slightly with stand age at the CH and ME sites, but no trend was found for the HJ site (Table 6). Heterotrophic respiration from soil and the forest floor accounted for 88% of annual turnover of

Table 5 Estimates of carbon stocks (kg C m^{-2} ground) in dead organic matter across three intensive sampling sites in Oregon

Site	Developmental stage	Age range (years)	Mineral soil C	Forest floor C	Woody detritus C*	Total necromass C	Necromass C/ecosystem C (fraction)
CH	Initiation	12–14	38 ± 12	0.39 ± 0.08	12 ± 4	50 ± 15	0.90 ± 0.02
	Young	22–40	39 ± 15	0.52 ± 0.14	18 ± 4	57 ± 11	0.78 ± 0.04
	Mature	45–52	28 ± 5	0.52 ± 0.13	8 ± 4	37 ± 6	0.54 ± 0.07
	Old	168–185	39 ± 7	0.56 ± 0.30	6 ± 3	46 ± 5	0.41 ± 0.06
HJ	Initiation	13–20	15 ± 1	0.54 ± 0.06	4 ± 1	19 ± 1	0.88 ± 0.02
	Young	39–70	15 ± 3	0.59 ± 0.13	6 ± 3	22 ± 2	0.64 ± 0.07
	Mature	143–166	11 ± 3	0.97 ± 0.24	4 ± 2	16 ± 5	0.30 ± 0.09
	Old	552–795	16 ± 3	1.00 ± 0.31	8 ± 3	25 ± 5	0.31 ± 0.07
ME	Initiation	9–23	8 ± 4	0.04 ± 0.02	4 ± 3	14 ± 6	0.94 ± 0.05
	Young	56–89	7 ± 2	0.05 ± 0.01	2 ± 1	9 ± 3	0.57 ± 0.02
	Mature	93–106	8 ± 1	0.08 ± 0.01	2 ± 1	12 ± 1	0.50 ± 0.12
	Old	190–316	5 ± 1	0.06 ± 0.02	2 ± 2	9 ± 3	0.33 ± 0.04

Values shown are means ± 1 standard deviation ($n = 3$).
*Woody detritus C includes dead roots.

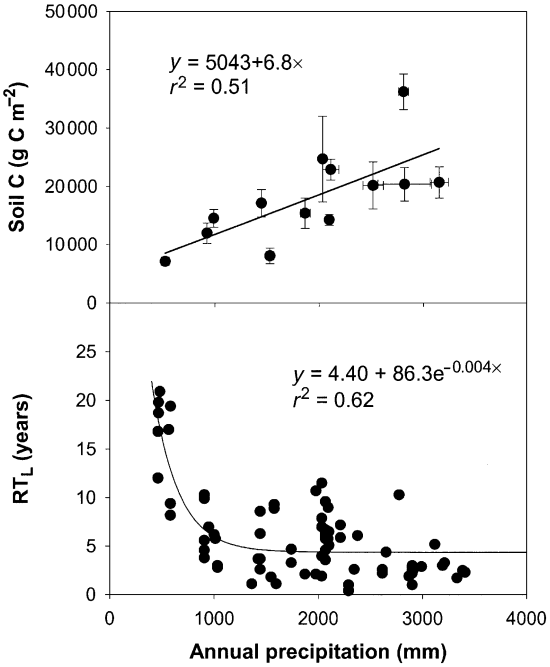

Fig. 3 Relationships between soil carbon stocks and mean residence time of the forest floor (RT_L) with annual precipitation across 13 study sites in the Pacific Northwest. Vertical and horizontal bars indicate $\pm$ 1 SE ($n = 12$ plots at the intensive sites and 6 at the extensive sites).

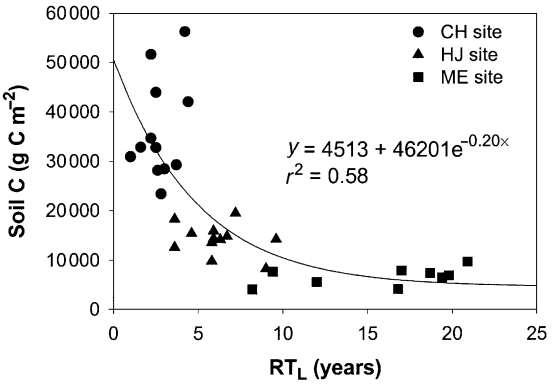

Fig. 4 Relationship between soil carbon and mean residence time of the forest floor (RT_L) across 36 plots at the intensive sites in Oregon.

total necromass carbon, which is consistent with our previous finding (Law *et al*., 2003). On average, the HJ site had the highest annual turnover rate of necromass carbon, and the CH site the lowest. Among the three intensive sites, the nitrogen-rich CH site differed significantly ($P \leq 0.05$) from the HJ and ME sites by having a relatively low proportion of LF soil carbon, but higher proportion of HF soil carbon (Table 7). The LF nitrogen concentration in the 0–20 cm soil depth ranged

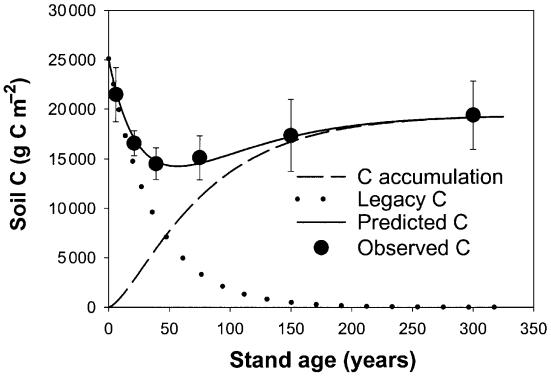

Fig. 5 Change in carbon stock, decomposition of legacy carbon, and carbon accumulation in mineral soils with stand age following stand-replacement disturbance across extensive sites of the Pacific Northwest. Predicted carbon stock is the sum of legacy carbon (modeled as an exponential decay function) and carbon accumulation from the current vegetation (Chapman–Richards function). Vertical bars indicate $\pm$ 1 SE ($n = 10$ plots).

from a mean of 0.94% at CH to 0.56% at HJ and 0.67% at ME. As shown in Fig. 7, both LF and HF differed significantly ($P \leq 0.0001$) among the three sites in the order of CH > HJ > ME. However, despite more than a twofold difference in total soil carbon, the LF carbon at the CH site was only 40% greater than that at the HJ site. The difference in total soil carbon between the CH and HJ sites predominantly resulted from a threefold difference in HF carbon. Across the three sites, HF accounted for 50–75% of total carbon in mineral soils in the 0–20 cm layer, with a significantly ($P \leq 0.0001$) greater proportion lower down in the soil profile (Table 7).

Simulations of temporal dynamics of soil carbon

Our simulations of soil carbon stock with stand age based on two independent functional processes, decomposition of legacy carbon, and carbon accumulation following stand-replacing disturbance, produced a remarkably tight fit to the average values of 10 extensive sites (Fig. 5). As in the observed pattern, modeled results showed that soil carbon stock declined initially with stand age until $\sim$ 50 years, driven by decomposition of legacy carbon, and that carbon accumulation from the current vegetation resulted in subsequent recovery in soil carbon stock until reaching an equilibrium between 150 and 200 years.

Discussion

Our results are in general agreement with those from a previous study on soil carbon stock in old-growth

Table 6 Estimates of heterotrophic respiration (R_h, g C m^{-2} ground yr^{-1}) across three intensive sampling sites in Oregon

Site	Developmental stage	Age range (years)	Soil R_h*	Woody detritus R_h†	Total R_h‡	Annual turnover rate of belowground C	Annual turnover rate of total necromass C
CH	Initiation	12–14	713 ± 68	61 ± 28	774 ± 96	0.015 ± 0.004	0.016 ± 0.004
	Young	22–40	643 ± 171	92 ± 21	734 ± 157	0.012 ± 0.003	0.013 ± 0.003
	Mature	45–52	676 ± 108	67 ± 22	743 ± 125	0.020 0.007	0.021 ± 0.006
	Old	168–185	967 ± 136	88 ± 21	1055 ± 115	0.023 0.002	0.023 ± 0.003
HJ	Initiation	13–20	1035 ± 121	58 ± 28	1093 ± 138	0.060 ± 0.008	0.058 ± 0.006
	Young	39–70	762 ± 66	83 ± 25	845 ± 42	0.041 ± 0.008	0.039 ± 0.005
	Mature	143–166	681 ± 78	90 ± 65	771 ± 116	0.055 ± 0.017	0.052 ± 0.012
	Old	552–795	546 ± 88	210 ± 57	756 ± 55	0.031 ± 0.009	0.031 ± 0.007
ME	Initiation	9–23	182 ± 7	58 ± 45	240 ± 39	0.017 ± 0.007	0.019 ± 0.006
	Young	56–89	199 ± 44	29 ± 18	228 ± 62	0.026 ± 0.007	0.026 ± 0.006
	Mature	93–106	302 ± 89	36 ± 16	338 ± 107	0.027 ± 0.009	0.028 ± 0.008
	Old	190–316	303 ± 32	28 ± 4	330 ± 36	0.041 ± 0.010	0.040 ± 0.010

Values shown are means ± 1 standard deviation ($n = 3$).
*Calculated as difference between annual soil respiration and annual root respiration.
†Decomposition from coarse and fine woody debris.
‡Sum of aboveground soil R_h and woody detritus R_h.

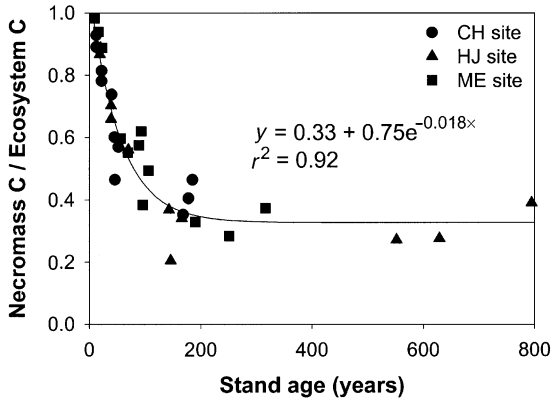

Fig. 6 Ratio of necromass carbon to ecosystem carbon as function of stand age across 36 plots at the intensive sites in Oregon.

forests of the Pacific Northwest (Remillard, 1999), where soil carbon varied with forest type (<5 to ~ 37 kg C m^{-2}). Overall, soil carbon stock of temperate coniferous forests of the Pacific Northwest cover a wide range of values observed in forest ecosystems around the world.

The differences in soil carbon among the sites could well be attributed to, among other factors, differences in site productivity. Site productivity has a direct control on biomass accumulation, which determines the size of detrital pool as the source of soil carbon.

Our results are in agreement with findings from many other studies that soil carbon increases with annual precipitation (i.e. Post *et al*., 1982; Jobbágy & Jackson, 2000; Zinke & Stangenberger, 2000; Schuur *et al*., 2001; Callesen *et al*., 2003). Schuur *et al*. (2001) attributed the increased soil carbon with annual precipitation in mesic to wet forests to a decrease in decomposition rates under limiting soil oxygen availability. Lack of oxygen limits decomposition of soil organic carbon in poorly drained soils due to reduced microbial activity (Davidson & Lefebvre, 1993; Schuur *et al*., 2001). This might explain the high soil carbon at the CH site where high rainfall and moist soil conditions persist throughout most of the year. In addition, the rates that carbon transfers from litter to mineral soils may also play a role in the effect of precipitation on carbon stock in mineral soils. This is supported by our finding that the residence time of litterfall decline with increasing precipitation. We suggest that precipitation affects total soil carbon by differentially affecting decomposition of soil and forest floor carbon: increased precipitation could slow down soil carbon decomposition by imposing oxygen-limiting conditions to microbial activity in mineral soils (Schuur *et al*., 2001), whereas it could accelerate decomposition of forest floor by enhancing microbial activity on the soil surface, where oxygen is rarely limiting except under waterlogged environments. Precipitation could also facilitate movement of particulate and soluble organic carbon from the forest floor into the soil profile.

Change in soil carbon stock with stand age has not been fully elucidated. Johnson & Curtis (2001) suggested that forest harvesting might have little or no

Table 7 Light (LF) and heavy density fractions (HF) of soil carbon across different stand ages at the intensive sampling sites in Oregon

Site	Plot ID	Stand age	Total soil C (%; 0–20 cm)	Total soil N (%; 0–20 cm)	C% of LF material	N% of LF material	LF (% of total soil C)		HF (% of total soil C)	
							0–20 cm	20–50 cm	0–20 cm	20–50 cm
CH	3	14	10.06	0.45	42.5	0.82	24.9 (5.7)	13.8 (2.0)	75.1 (5.7)	86.2 (2.0)
	7	45	11.90	0.58	43.2	0.88	30.8 (15.9)	17.7 (6.1)	69.2 (15.9)	82.3 (6.1)
	11	168	14.50	0.69	41.2	1.12	24.2 (11.5)	12.8 (5.0)	75.8 (11.5)	87.2 (5.0)
	Mean		12.33	0.57	42.3	0.94	26.6	14.7	73.4	85.3
HJ	13	19	5.85	0.18	40.1	0.52	52.0 (9.1)	32.7 (18.8)	48.0 (9.1)	67.3 (18.8)
	21	166	6.85	0.20	39.6	0.62	42.3 (9.1)	31.2 (8.8)	57.7 (9.1)	68.8 (8.8)
	24	629	3.46	0.12	38.6	0.53	35.3 (5.6)	22.2 (3.4)	64.7 (5.6)	77.8 (3.4)
	Mean		5.39	0.17	39.4	0.56	43.2	28.7	56.8	71.3
ME	25	23	2.01	0.07	37.5	0.73	38.2 (7.9)	33.1 (1.2)	61.8 (7.9)	66.9 (1.2)
	30	89	2.12	0.07	33.1	0.62	36.3 (8.7)	33.3 (2.7)	63.7 (8.7)	66.7 (2.7)
	34	190	1.47	0.05	37.2	0.67	33.5 (6.5)	30.3 (5.6)	66.5 (6.5)	69.7 (5.6)
	Mean		1.86	0.06	35.9	0.67	36.0	32.2	64.0	67.8

Standard deviations are shown in parentheses ($n = 3$ composite samples).

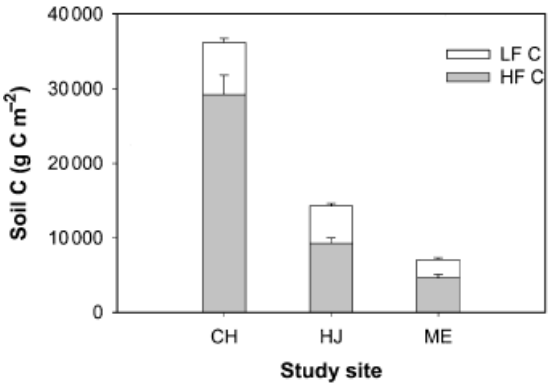

Fig. 7 Soil carbon stock in light (LF) and heavy density fractions (HF) at the intensive sites in Oregon. Vertical bars indicate ± SE ($n = 12$ plots).

effect on soil carbon, and that wildfire resulted in higher soil carbon due to sequestration of charcoal and recalcitrant, hydrophobic organic matter and the post-fire in-growth of nitrogen-fixing vegetation. Fire affects the molecular composition of soil carbon, and converts soil organic carbon to more degradation-resistant charcoal (Czimczik *et al*., 2003). Except for the old forests, the primary mode of stand-replacing disturbance at the intensive sites was forest harvest, whereas we know less about stand history for the younger stands at the extensive sites. Results from our study showed inconsistent patterns of soil carbon with stand age among sites.

There was no apparent trend in soil carbon stocks (Table 5) and annual heterotrophic respiration (Table 6; Law *et al*., 2003) in soils and in various detrital pools in relation to stand age, possibly because of the effects of other factors such as topography and soil depth at the sites.

The low rate of annual turnover at the CH site could be partially attributed to the high annual precipitation that impeded soil carbon decomposition (Schuur *et al*., 2001), which, together with the high NPP of the forest types, explains a greater accumulation of total necromass carbon at the CH site compared with the other two sites (Table 6).

The turnover times of soil carbon are controlled, to a large extent, by the relative size of labile and nonlabile pools interacting with climatic and edaphic factors (Davidson *et al*., 2000). Heavy density fractions of mineral soil carbon are slower in turnover times than light density fractions (Sollins *et al*., 1996; Swanston *et al*., 2002). Our analysis of carbon density fractions in mineral soils on subsets of plots at the three intensive sites showed evidence of spatial and temporal variation. Our results agree with the finding by Neff *et al*. (2002) that high soil nitrogen availability has differential effects on LF and HF. Increased N accelerates decomposition of LF while further stabilizing HF.

Previous work by Cromack *et al*. (1999), conducted in a coastal Oregon Douglas-fir plantation intermixed with red alder, showed that the light fraction for the 0–15 cm mineral soil depth accounted for a mean of 13.4% of the <2 mm size fraction soil mass, had a carbon concentration of 43.3%, and accounted for 40.0% of the total soil C mass in the <2 mm size fraction. We obtained a similar carbon concentration in the LF material in this study (Table 7). The much higher N concentration of 1.84% N in the light fraction of the 0–15 cm soil depth at Waldport, relative to the CH data in our study (0.94% in 0–20 cm depth), may be due in

part to the previous site disturbance and subsequent secondary succession at Waldport, including clear cutting and broadcast burning in 1969–1970, followed by Douglas-fir replanting, natural colonization by red alder (N-fixer) and salmonberry, and then partial herbicide treatment during 1980. Although red alder is common on coastal Oregon, our study plots do not contain the species. It should be noted that the soil fractionation work by Cromack *et al*. (1999) was conducted using the older methodology of density separation with NaI (Spycher *et al*., 1983), rather than the newer methodology using sodium polytungstate as used in our study. Nevertheless, the two methods should provide comparable results.

Although the two critical parameters, k_G and r, for describing soil carbon accumulation with stand age were derived from total biomass carbon, the model appeared to be functionally correct when the value of soil carbon at steady state (i.e. in old-growth forests) was used to constrain the maximum of the growth function. This suggests that soil carbon accumulation with stand age depends strongly on biomass carbon, which is controlled by site productivity and mortality rates.

Three factors are important in simulating the temporal dynamics of soil carbon storage: initial carbon stock (legacy carbon), rates of decomposition, and rates of carbon accumulation from the current vegetation. Legacy carbon is determined by the previous vegetation and the mode and intensity of disturbance, and the rates of decomposition are influenced by both climatic and edaphic factors, whereas the rates of carbon accumulation depend on the rates of vegetation recovery and productivity following stand-replacement disturbances. The different patterns of modeled soil carbon stocks with stand age across sites could be explained by differences in soil carbon turnover rates and site productivity under the influence of climate.

Acknowledgements

This study was funded by US EPA National Center for Environmental Research (NCER) Science to Achieve Results (STAR) Program (Grant #R-82830901-0). We thank William Austin and Sandy Lovelady at OSU's Central Analytical Lab for soil chemical and particle size analysis. We gratefully acknowledge the district offices of US Forest Service and Bureau of Land Management (BLM) in Oregon and Washington for permission and assistance to access to the study sites. We thank Kermit Cromack, Mark Harmon, Phillip Sollins, and Richard Waring for constructive comments and valuable discussions that helped greatly to improve the paper. Acknowledgements of field sampling and data collection to: Jesse Bablove, Jason Barker, Aaron Domingues, Isaac Emery, Nathan Gehres, Erica Lyman-Holt, Darrin Moore, Adam Pfleeger, Lucia Reithmaier, Nathan Strauss.

References

Callesen I, Liski J, Raulund-Rasmussen K *et al*. (2003) Soil carbon storage in Nordic well-drained forest soils – relationships with climate and texture class. *Global Change Biology*, **9**, 358–370.

Cromack K, Miller RE, Helgerson OT *et al*. (1999) Soil carbon and nutrient in a coastal Oregon Douglas-fir plantation with red alder. *Soil Science Society of America Journal*, **63**, 232–239.

Czimczik CI, Preston CM, Schmidt MWI *et al*. (2003) How surface fire in Siberian Scots pine forests affects soil organic carbon in the forest floor: stocks, molecular structure, and conversion to black carbon (charcoal). *Global Biogeochemical Cycles*, **17**, 1020, doi:10.1029/2002GB001956..

Davidson EA, Lefebvre PA (1993) Estimating regional carbon stocks and spatially covarying edaphic factors using soil maps at three scales. *Biogeochemistry*, **22**, 107–131.

Davidson EA, Trumbore SE, Amundson R (2000) Soil warming and organic carbon content. *Nature*, **408**, 789–790.

Eswaran H, Van Den Berg E, Reich P (1993) Organic carbon in soils of world. *Soil Science Society of America Journal*, **57**, 192–194.

Franklin JF, Dyrness CT (1973) *Natural vegetation of Oregon and Washington*. *Pacific Northwest forest and range experiment station*. USDA Forest Service General Technical Report PNW 8.

Gee GW, Bauder JW (1986) Particle-size analysis. In: *Methods of Soil Analysis, Part 1 – Physical and Mineralogical Methods. Agronomy Monograph 9*, 2nd edn (ed. Klute A), pp. 383–411. Soil Science Society of America, Madison, WI.

Gholz HL, Grier CC, Campbell AG *et al*. (1979) *Equations for estimating biomass and leaf area of plants in the Pacific northwest*. FRL Research Paper 41. School of Forestry, Oregon State University, OR

Giardina CP, Ryan MG (2000) Evidence that decomposition rates of organic carbon in mineral soil do not vary with temperature. *Nature*, **404**, 858–861.

Guo LB, Gifford RM (2002) Soil carbon stocks and land use change: a meta analysis. *Global Change Biology*, **8**, 345–360.

Harmon ME, Sexton J (1996) *Guidelines for measurements of woody detritus in forest ecosystems*. Publication No. 20, US LTER Network Office, University of Washington, Seattle, WA.

Homann PS, Sollins P, Fiorella M *et al*. (1998) Regional soil organic carbon storage estimates for western Oregon by multiple approaches. *Soil Science Society of America Journal*, **62**, 789–796.

Janisch JE, Harmon ME (2002) Successional changes in live and dead wood carbon stores: implications for ecosystem productivity. *Tree Physiology*, **22**, 77–89.

Jobbágy EG, Jackson RB (2000) The vertical distribution of soil organic carbon and its relation to climate and vegetation. *Ecological Applications*, **10**, 423–436.

Johnson DW, Curtis PS (2001) Effects of forest management on soil C and N storage: meta analysis. *Forest Ecology and Management*, **140**, 227–238.

Law BE, Ryan MG, Anthoni PM (1999) Seasonal and annual respiration of a ponderosa pine ecosystem. *Global Change Biology*, **5**, 169–182.

Law BE, Sun OJ, Campbell J *et al*. (2003) Changes in carbon storage and fluxes in a chronosequence of ponderosa pine. *Global Change Biology*, **9**, 510–524.

Law BE, Thornton PE, Irvine J *et al*. (2001) Carbon storage and fluxes in ponderosa pine forests at different developmental stages. *Global Change Biology*, **7**, 755–777.

Law BE, Turner D, Lefsky M *et al*. (2004) Carbon fluxes across regions: observational constraints at multiple scale. In: *Scaling and Uncertainty Analysis in Ecology* (eds Wu J, Jones B, Li H, Loucks OL), Columbia University Press, New York.

Neff JC, Townsend AR, Gleixner G *et al*. (2002) Variable effects of nitrogen additions on the stability and turnover of soil carbon. *Nature*, **419**, 915–917.

Parton WJ, Scurlock JMO, Ojima DS *et al*. (1995) Impact of climate change on grassland production and soil carbon worldwide. *Global Change Biology*, **1**, 13–22.

Post WM, Emanuel WP, Zinke PJ *et al*. (1982) Soil carbon pools and world life zones. *Nature*, **298**, 156–159.

Remillard SM (1999) *Soil carbon and nitrogen in old-growth forests in western Oregon and Washington*. MS thesis, Oregon State University, Corvallis, USA.

Ryan MG, Lavigne MB, Gower ST (1997) Annual carbon cost of autotrophic respiration in boreal forest ecosystems in relation to species and climate. *Journal of Geophysical Research, BOREAS Special Issue*, **102**, 28871–28884.

Rustad LE, Campbell JLGCTE-NEWS *et al*. (2001) A meta-analysis of the response of soil respiration, net nitrogen mineralization, and aboveground plant growth to experimental ecosystem warming. *Oecologia*, **126**, 543–562.

Schuur EAG, Chadwick OA, Matson PA (2001) Carbon cycling and soil carbon storage in mesic to wet Hawaiian montane forests. *Ecology*, **82**, 3182–3196.

Sollins P, Homann P, Caldwell BA (1996) Stabilization and destabilization of soil organic matter: mechanisms and controls. *Geoderma*, **74**, 65–105.

Spycher G, Sollins P, Rose SL (1983) Carbon and nitrogen in the light fraction of a forest soil: vertical distribution and seasonal patterns. *Soil Science*, **135**, 79–87.

Strickland TC, Sollins P (1987) Improved method for separating light- and heavy-fraction organic material from soil. *Soil Science Society of America Journal*, **51**, 1390–1393.

Swanston CW, Caldwell BA, Homann PS *et al*. (2002) Carbon dynamics during a long-term incubation of separate and recombined density fractions from seven forest soils. *Soil Biology and Biochemistry*, **34**, 1121–1130.

Torn MS, Trumbore SE, Chadwick OA *et al*. (1997) Mineral control of soil organic carbon storage and turnover. *Nature*, **389**, 170–173.

Wang CK, Bond-Lamberty B, Gower ST (2003) Carbon distribution of a well- and poorly-drained black spruce fire chronosequence. *Global Change Biology*, **9**, 1066–1079.

Zinke PJ, Stangenberger AG (2000) Elemental storage of forest soil from local to global scales. *Forest Ecology and Management*, **138**, 159–165.